Supporting Information

Schwerdt et al. 10.1073/pnas.1713756114

SI Materials and Methods

Fabrication of Sensors. The CF sensors were composed of a front end sensor, which is equivalent to rodent-applied sensors (3, 4), and an elongated support shaft through which the sensor is threaded to allow ease of manual handling and implantation toward deep (15–25 mm) brain structures in the monkeys (Fig. S9). The front end sensor was fabricated by first cleaving a 90-μm-diameter fused-silica capillary (TSP020090; Polymicro) to a length of 2–3.5 cm using a carbide cutter and cutting 7-μm-diameter CF bundles (C 005722; Goodfellow) into lengths of 4.5–5 cm using scissors. These parts were soaked in a dish of isopropanol, where cotton-tipped applicators were used to thread the CF into a capillary (Fig. S8*A*). The threaded capillaries were removed from the dish and left to dry in air overnight or by heating on a hot plate at 80 °C for 15 min. After drying, structural epoxy (14250; Devcon) was applied at the base of the extruding carbon fiber and the fiber was pulled into the capillary from the other end to allow epoxy to permeate and fill the capillary. After the epoxy had solidified, the remaining CF was cut with scissors so that a 150- to 300-μm-long CF remained protruding from the epoxy (Fig. S8*A*). The CF protruding out of the other side of the capillary was trimmed so that a 2- to 5-mm tail remained. The support shaft was fabricated by threading a microelectrode (FHC, UEWLCDVM1N1X) through a 164-μm-diameter and 8-cm-long fused-silica capillary (TSP100170; Polymicro) (Fig. S8*B*). The microelectrode was scraped at the tip to expose 5 mm of conductive surface. The conductive tip was painted with silver epoxy (H20S; Epo-tek) along a length of 5–15 mm from the tip and pulled into the capillary until the tip was ∼1-mm submerged from the end of the capillary (Fig. S8*B*). The CF tail of the front end sensor was aligned to the larger capillary and the tail, and smaller capillary were inserted into the larger capillary until 5–10 mm of the smaller capillary had been inserted (Fig. S8*C*). The silver epoxy was cured by placing threaded assemblies onto a hot plate at 100 °C for >45 min. A thin layer of the structural epoxy was applied onto the base of the threaded smaller capillary to permeate gaps between the larger and smaller capillaries and to ensure sealing and insulation. The structural epoxy was also applied between the threaded microelectrode and larger capillary at the opposite end of the CF to further strengthen mechanical integration between the electrode and the larger capillary (Fig. S8*C*).

Electrochemical Recording. The FSCV recording system was obtained from Scott B. Ng-Evans, University of Washington, Seattle, WA. It displays noise of ∼0.1 nA (measured with a dummy tissue-emulating circuit consisting of a series capacitor of 3.3 nF and resistor of 10 kΩ, with digital filtering turned off and standard recording parameters), dynamic range of ±2,000 nA, and samples per scan of 175. The scan refers to the period in which a ramping triangular voltage is applied to the sensor to generate and detect electrochemical current. Each scan is applied at 100-ms intervals. Current recorded at each scan were concatenated to create background-subtracted signals of the change in current along the applied voltages versus time. These were visualized in color plots (Figs. 2*A*, 3*A*, 4 *A* and *B*, and 5 *A*–*F*, and Figs. S2, S3, and S6*A*), which display current in a nonlinear color-scale, voltage in the *y* axis, and time in the *x* axis. At each sample time (i.e., at each scan), the CV (current vs. voltage plot) is assessed to identify the voltages at which current increases or decreases, which usually confer oxidation or reduction, respectively, of an electroactive substance (Fig. 3*B*). The redox potentials or voltages at which peak current changes occur are −0.2 and 0.6 V for dopamine. Dopamine concentration change is linearly proportional to the oxidation current (i.e., current at the oxidation potential). However, current variations can also occur at voltages outside of the dopamine redox potentials, and these interfering currents are related to other molecular or ionic changes at the sensor (23). To ensure that the measured current is mostly related to dopamine redox without significant interference, correlation to dopamine standards as well as principal component regression analyses are required and were performed (*Materials and Methods*). Through these corroboration procedures, current measurements could be converted to apparent change in dopamine concentration ($[DA]_a$). In all measurements, we implemented a digital Gaussian filter. All analyses were performed in Matlab (Mathworks, Matlab 2016a).

For in vitro measurements, a triangular waveform ramping from −0.4 to 1.3 to −0.4 V at 400 V/s was applied to the CF sensors for each scan at a cycle frequency of 10 Hz and a hold potential of −0.4 V between scans. For in vivo measurements, a positive D.C. offset was applied (0.1–0.2 V) to compensate for the decreased reference potentials commonly observed in vivo (4) that would effectively reduce sensitivity. Before recording, the CF sensors were conditioned by applying the same ramp at a cycle frequency of 10 Hz for 60 min to stabilize changes in background current. For all measurements, the reference (ground) was connected to Ag/AgCl electrodes implanted in white matter (>5 mm away from CF sensors) or on the dural surface that were also tied to epidural stainless steel electrodes. However, in M3, the reference was connected only to epidural stainless steel electrodes.

In Vitro Characterization of Sensors. CF sensors were tested in vitro using a flow cell to determine sensitivity to dopamine and to create CV standards. Phosphate-buffered saline (PBS) buffer and solutions of 0.25, 0.5, and 1 μM dopamine hydrochloride (H8502; Sigma-Aldrich) dissolved in PBS were infused separately into the flow cell by electronic actuation of a sample injection valve (Model 22Z; Valco). Movement-induced CVs were acquired during movement from intrastriatal electrodes that did not display CVs representative of dopamine (i.e., dopamine redox current peaks) during the entire recording session or electrodes whose CF sensing tips remained inside the guide tube and in the white matter region at least 1-mm dorsal to the striatum. The movement-induced current is caused by physical displacement of the electrode and resulting changes in the electrical properties of the electrode-tissue interface, electrostatic influence, or triboelectric charging. Background-drift CVs were acquired by actively recording from in vitro electrodes in dopamine-free PBS solutions where current changes steadily occur over time (>30 s) due mostly to changes in the surface properties of the CF sensing interface and applied voltages.

Implantation Procedures. All CF sensors were implanted through a 0.41-mm outer-diameter guide tube (27G-XTW-'A'-bevel; Connecticut Hypodermics) that protected the delicate 7-μm CF at their tips. The guide tubes penetrated the dura mater and traveled 5–10 mm until they were estimated to be 2–5 mm above the targeted striatal regions. Threaded CF sensors were slowly lowered out of the guide tubes using a micromanipulator to allow approaching targets 5–13 mm below the guide tube tips. Upon reaching targets, sensors were fixed to the microdrives and guide tubes were slowly removed from the brains. In monkeys

M1 and M3, three to five chronic stimulation electrodes were secured 3–5 mm above targeted SNc/VTA regions whose recorded spike firing rates were shown to be phasically influenced in response to reward-related cues (13). These electrodes were implanted before implantation of chronic CF sensors. The stimulation electrodes were lowered during dopamine recording sessions by rotating screw terminals on the microdrive shuttles. In M2, four stimulation electrodes were chronically implanted after chronic CF sensor implantation. Three of these chronic electrodes were placed with the same electrophysiological mapping procedures used for M1 and M3. One of these chronic stimulation electrodes, along with three acute stimulation electrodes, were implanted based on stimulation-induced dopamine release amplitude measured from acute CF sensors in the putamen. All implanted devices were subjected to low temperature hydrogen peroxide plasma (STERRAD; Advanced Sterilization Products), except for CF sensors, which were treated by immersion in 70% isopropanol [(vol/vol) in water] for >2 h followed by air-drying and exposure to UV (UV-C) light.

Stimulation of Dopamine-Containing Neurons or Their Axons. Current-controlled stimulation consisted of 18 biphasic pulses (1 ms per pulse) with an amplitude of 150–320 μA and a frequency of 200 Hz, as supplied by a stimulus isolator (A365; WPI) that was triggered by the software of the recording instrumentation. We used 125-μm-diameter Pt-Ir microelectrodes with tip impedances of 80–200 kΩ (FHC) for stimulation. The stimulation was usually delivered in intervals of 3–5 min to avoid depleting dopamine terminals. Regions at which stimulation triggered striatal dopamine release were located by lowering microelectrodes along MRI-estimated trajectories (Fig. S1) to electrophysiologically identify sites of enhanced electrical neural activity during reward-predictive cues or by directly stimulating and identifying regions triggering detectable dopamine with sensors acutely implanted in the striatum. Changes in stimulation-induced dopamine over time (in the same session) are shown as maximum dopamine oxidation current changes measured in each stimulation trial (Fig. 2*C*) with error bars indicating SD. Changes in drug-modulated stimulation-induced are calculated by averaging over four to seven stimulation trials before and after drug administration (Fig. 2 *D* and *E* and Fig. S3 *C*–*F*). Only trials during which stimulation produced a signal that could be identified as dopamine (*Materials and Methods*) were included in these calculations. Because postdrug stimulation-induced dopamine changes were highly variable compared with baseline (predrug) amplitudes, only postdrug signals greater than 1 SD of the baseline signal were used.

Fate of Implanted Probes. The most frequent failure mode of implanted probes was attributed to mechanical breakage of the CF sensor during user handling and rewiring of connectors within chamber housing. Mill-Max connectors at the end of the CF sensors were frequently reconfigured to connect to different pins on the Mill-Max connector of the headstage. Significant strains at the base of the silica tube, where the tungsten wire protrudes out, could lift the tungsten/silver–epoxy interface from the CF (Fig. S8), causing an electrical disconnect and premature sensor failure. This strain was most likely induced when the user gripped the wires during sudden animal head movement. Repeated strain of the tungsten wire could also fatigue fracture near to the silica insulation that could not subsequently be reconnected. Three of the six implanted probes in monkey M1 broke due to these issues before they could be used. Probes cn1, cn2, and cn3 were used, respectively, until 68, 126, and 176 d postimplant, when they experienced a mechanical failure. Seventeen of 19 probes in M2 progressively failed, but the exact date that these failures occurred could not be noted because the performance of each probe was not evaluated in each session. All probes except cl7 and p6 were observed to be nonfunctional on postimplant day 179.

Histology. Brains were fixed for immunohistochemical analysis after electrodes had been implanted for 6–12 mo to assess location of implants (Fig. S9). We located stimulation electrodes in monkeys M1 and M3, which were within regions with the expression of tyrosine hydroxylase (TH) (Fig. S9 *A* and *B*). We located CF sensors in M1, which were implanted in the striatum (Fig. S9*C*). The monkeys were deeply anesthetized with an overdose of sodium pentobarbital and were perfused with 0.9% saline followed by 4% paraformaldehyde in 0.1 M phosphate buffer (PB). Brains were kept in 4% buffered paraformaldehyde for 3 d, and then the electrodes were withdrawn. Then brains were blocked and stored in 25% glycerol in 0.1% sodium azide (438456; Sigma) in 0.1 M PB at 4 °C. Blocks containing the striatum and SNc were frozen in dry ice and cut on a sliding microtome at 40 μm in the transverse plane. Sections were stored in 0.1% sodium azide in 0.1 M PB. Selected sections were used for immunofluorescence staining and imaged with an automatized slide scanner (TissueFAXS Whole Slide Scanner; TissueGnostics) with 10× objectives.

Immunohistochemistry. For immunofluorescence staining, sections were rinsed three times for 2 min in 0.01 M PBS containing 0.2% Triton X-100 (Tx) (T8787; Sigma-Aldrich), and were incubated in tyramide signal amplification (TSA) blocking reagent (FP1012; PerkinElmer) in PBS-Tx (TSA-block) for 1 h. Then the sections were incubated with primary antibody solutions containing chicken antiglial fibrillary acidic protein (GFAP) (1:500; ab4674; Abcam) and rabbit anti-TH (1:4,000; ab112-100; Abcam) in TSA-block for 24 h at 4 °C for GFAP and TH double staining. We used chicken anti-GFAP (1:500, ab4674; Abcam) and mouse anti-K channel interacting protein (KChIP) (1:200; #75-003; University of California, Davis/NIH NeuroMab Facility) for GFAP and KChIP double staining. After primary incubation, the sections were rinsed three times for 2 min in PBS-Tx, and then were incubated for 1 h in the secondary antibody solution containing biotinylated goat anti-rabbit (1:400; BA-1000; Vector Laboratories) in TSA-block for TH staining. We used biotinylated goat anti-mouse (1:400; BA-9200; Vector Laboratories) for KChIP staining. After 3 × 2 min rinses in PBS-Tx, they were incubated in TSA-block containing anti-chicken Alexa Fluor 488 (1:300; A11039; Life Technologies) and Streptavidin 647 (1:2,000; A32357; Life Technologies) for 1 h. Then the sections were rinsed three times for 2 min in 0.1 M PB, and mounted onto glass slides and coverslipped with ProLong antifade reagent (P36930; Life Technologies).

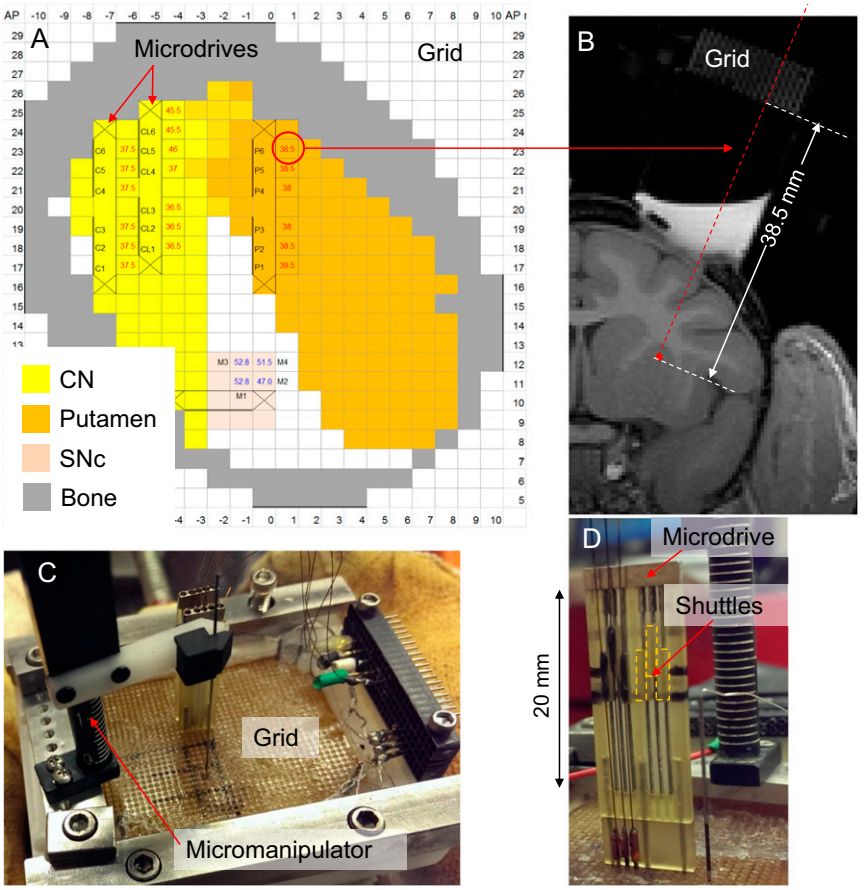

Fig. S1. Modular chamber interface. (*A*) Chamber-mounted grid layout for monkey M2, displaying grid holes (individual square cells) and outlines of targeted striatum regions for chronic CF sensors (red numbers indicating targeted depth as measured from the bottom of grid) projecting below grid plane (23° tilted in coronal plane). Color codes are shown at bottom left. (*B*) Coronal MRI (T1, 0.5-mm resolution) of estimated plane at antero-posterior (AP) 23 mm, showing an example of electrode trajectory within putamen. (*C*) Top of chamber and grid with mounted micromanipulator for acute manipulation and implantation of CF sensor. (*D*) Microdrive installed on grid with shuttles holding chronically implanted CF sensors.

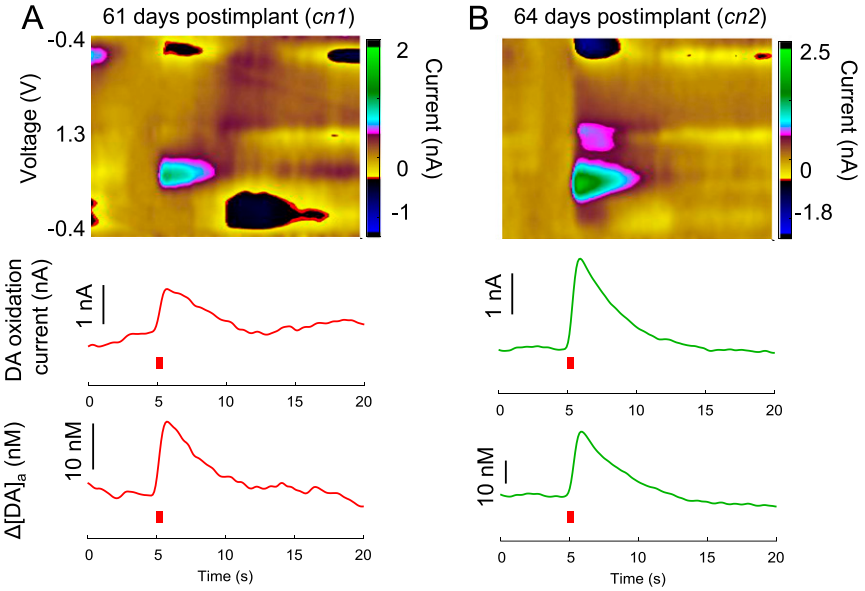

Fig. S2. Measurements of dopamine release evoked by electrical stimulation in chronic recordings from monkey M1. Representative background-subtracted current (*Top*), dopamine (DA) oxidation current (*Middle*), and computed apparent dopamine concentration change $[DA]_a$ (*Bottom*) as evoked by electrical stimulation (at 5 s, red rectangle indicates stimulation period) measured on postimplant day 61 from probe cn1 (*A*) and on postimplant day 64 from probe cn2 (*B*).

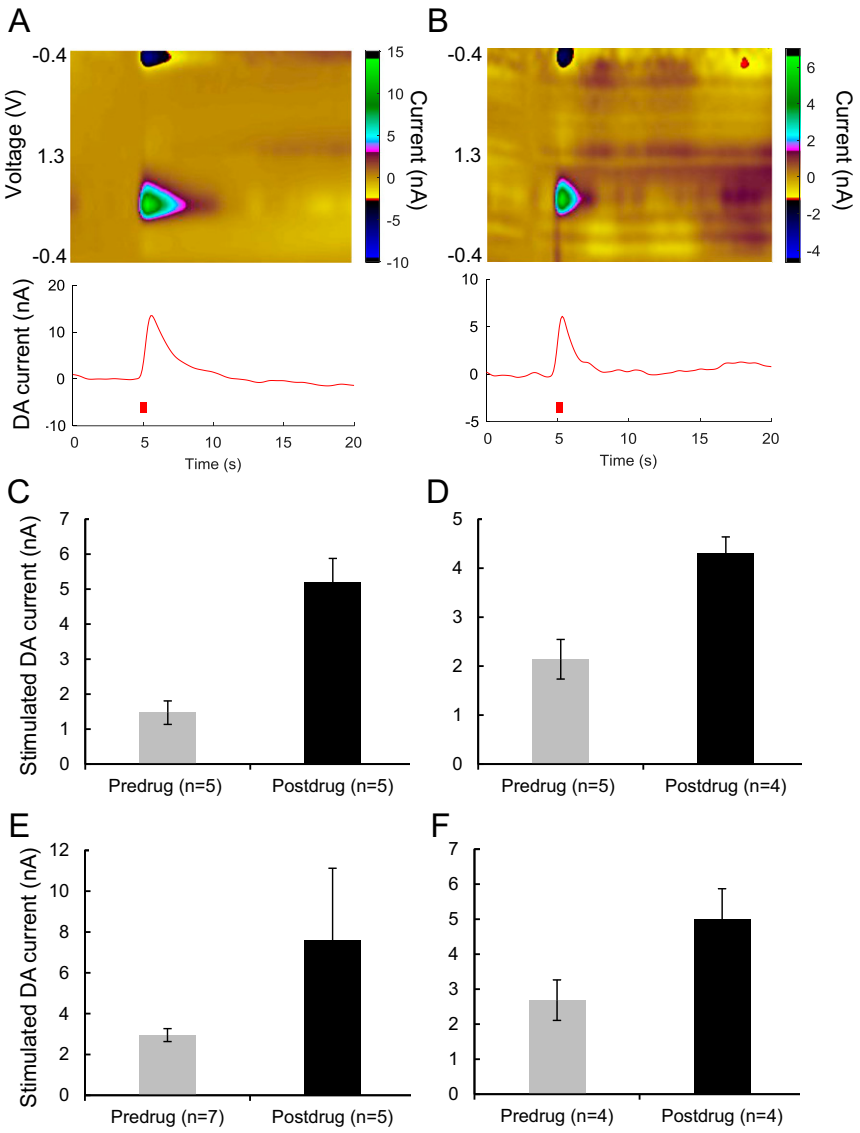

Fig. S3. Acute measurements of stimulation-evoked dopamine and changes with raclopride treatment. (*A* and *B*) Representative background-subtracted current (*Upper*) and computed dopamine concentration change (*Lower*) as evoked by electrical stimulation (at 5 s, red rectangle) measured from an acutely implanted sensor in the putamen of monkeys M3 (*A*) and M2 (*B*). (*C*–*F*) Average peak stimulation evoked dopamine measured in the caudate nucleus of M1 (*C*) and in the putamen of M1 (*D*), M3 (*E*), and M2 (*F*), before and after raclopride treatment. Error bars represent SD.

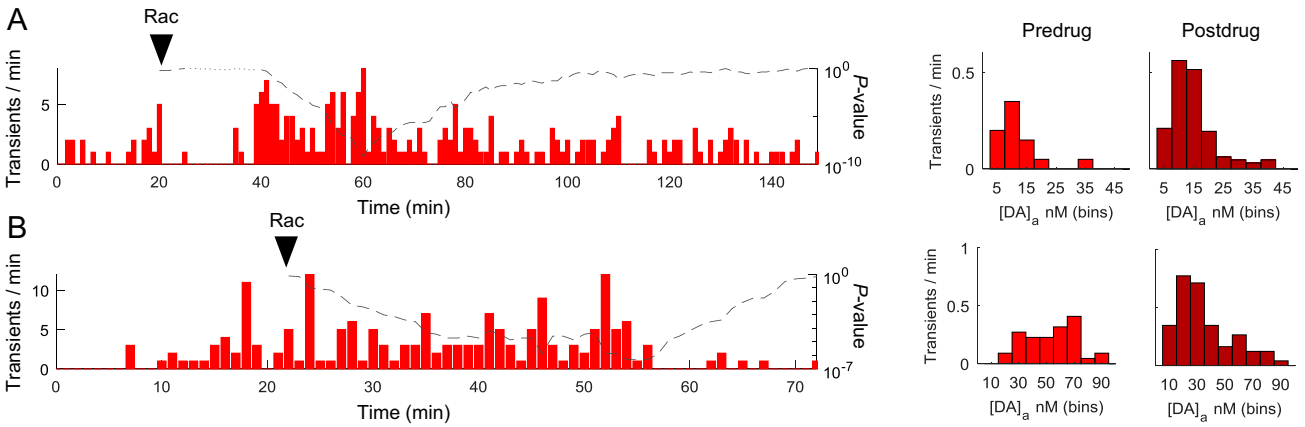

Fig. S4. Drug-modulated dopamine transients measured from acutely implanted sensors. (*A* and *B*) Frequency of detected dopamine signals (1 min bins, *Left y* axis) over time from a continuous recording in putamen of monkeys M1 (*A*) and M2 (*B*, *Left*), and monkey distribution of detected dopamine concentration changes and their frequencies from data in *A*, *Right*, shown as in Fig. 4 *C* and *D*.

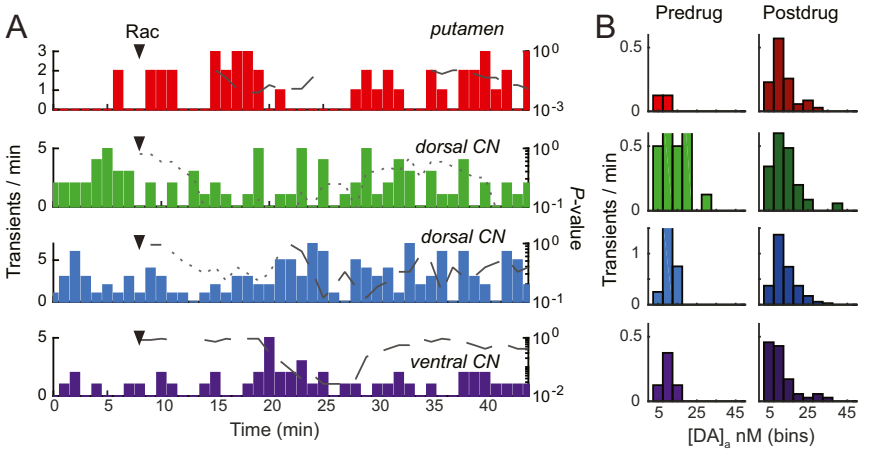

Fig. S5. Drug-modulated dopamine transients measured simultaneously from four striatal sites, from top to bottom: dorsal putamen (p1), posterior dorsal CN (cl1), anterior dorsal CN (cl3), and ventral CN (cl5) of monkey M2 on postimplant day 99. (*A*) Frequency of detected dopamine signals (1-min bins, *Left y* axis) over time from a continuous 43 min recording as in Fig. 4 *C* and *D*. (*B*) Distribution of detected dopamine concentration changes and their frequencies from data in *A*.

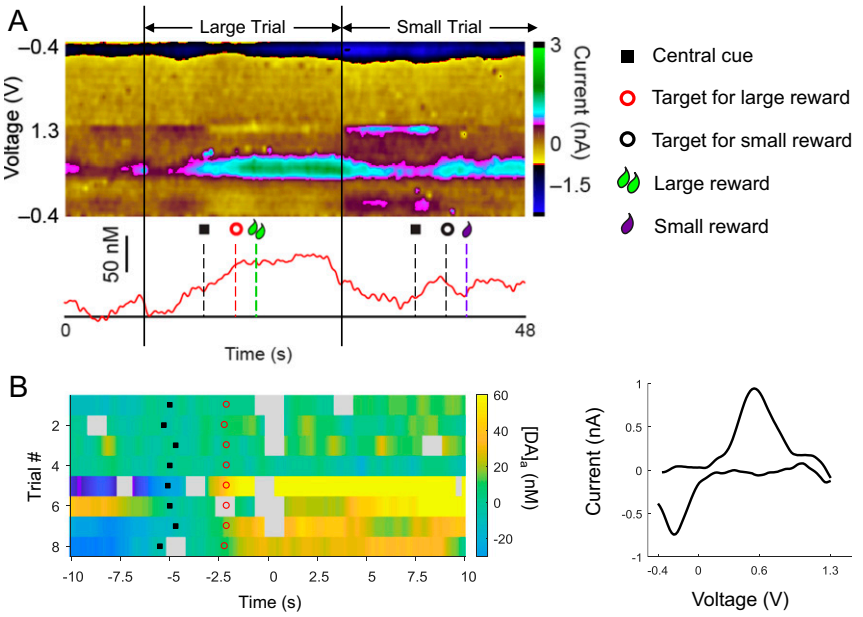

Fig. S6. Changes in dopamine during trials with small and large reward in 1DR task as measured from an acutely implanted sensor in putamen in monkey M2. (*A*) Representative measurement during a large-reward trial followed by a small-reward trial. The *Upper* panel is a color plot of the voltage-dependent background-subtracted data, and the *Lower* panel is the extracted apparent dopamine concentration. (*B*) Changes in dopamine recorded during individual large-reward trials (*y* axis) relative to reward delivery (time 0). Trials are sorted based on their actual sequence. Gray represents periods displaying extraneous CVs within each trial. Average CV obtained from dopamine-conferred signals across trials shown at right.

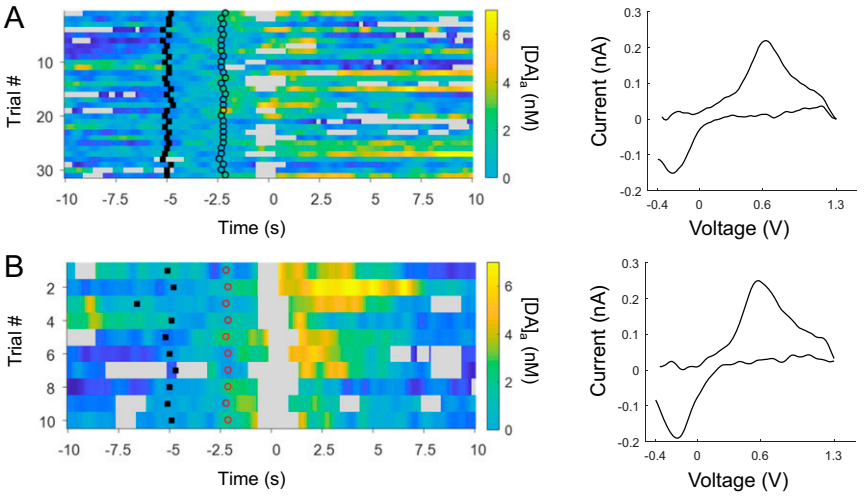

Fig. S7. Trial-by-trial changes in dopamine during small- and large-reward trials measured from a chronically implanted sensor (data shown in Fig. 5*G*). Trial-by-trial changes in dopamine during trials with small (*A*) and large (*B*) rewards are shown as in Fig. S6*B*.

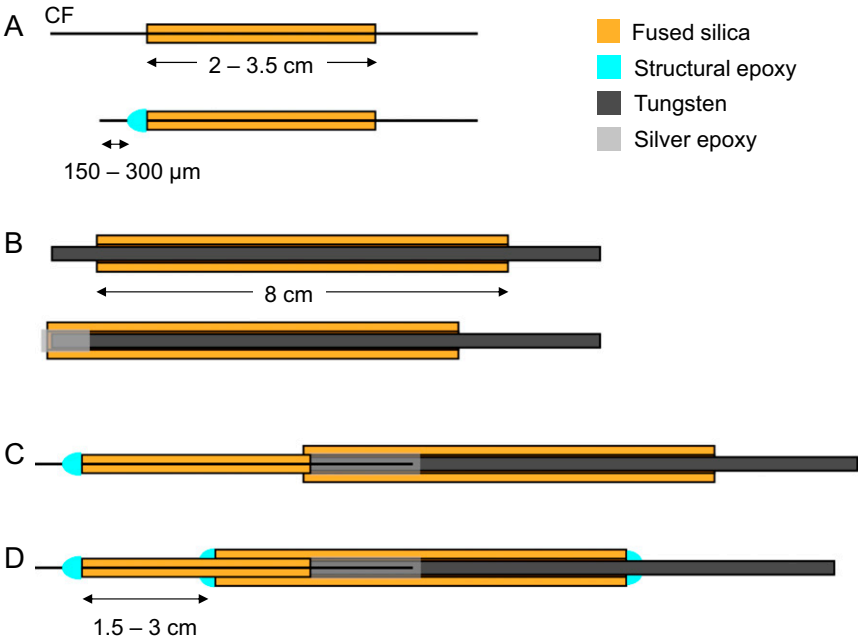

Fig. S8. Fabrication process for CF sensors. (*A*) Front end sensor fabrication by threading a 7-μm-diameter CF in a 90-μm-diameter fused-silica capillary (*Upper*) and by applying structural epoxy at the tip of the capillary to seal the CF. The CF is trimmed to an exposed length of 150–300 μm (*Lower*). (*B*) Support shaft fabrication by threading a microelectrode through a 164-μm-diameter fused-silica capillary (*Upper*) and by applying silver epoxy at the electrode tip and pulling into the capillary (*Lower*). (*C*) Front end sensor inserted into the support shaft. (*D*) Structural epoxy applied between capillaries and threaded microelectrode to seal and strengthen integration between parts.

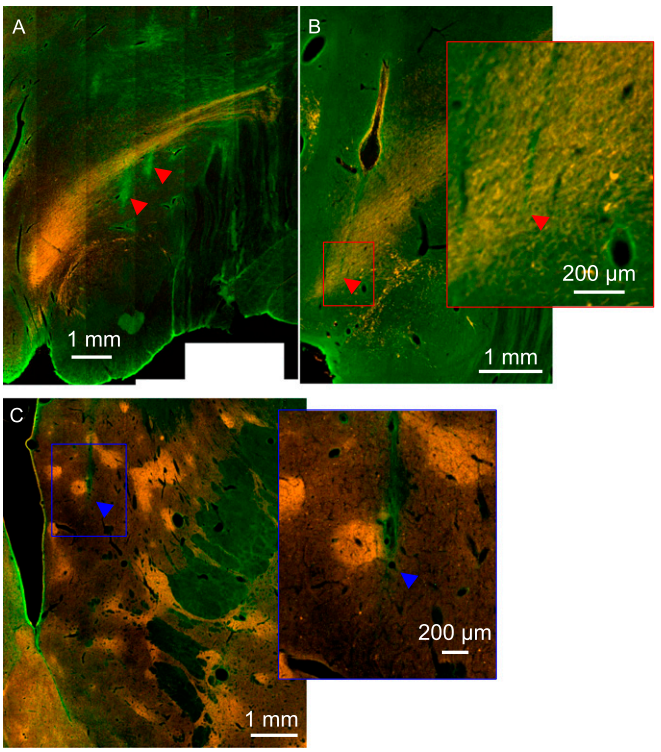

Fig. S9. Immunohistochemical analysis of SNc/VTA stimulation sites and striatal recording sites. (*A* and *B*) Coronal section of midbrain in monkeys M3 (*A*) and M1 (*B*), displaying targeted TH-expressing regions and the putative tips and tracks of stimulation electrodes indicated by higher GFAP expression (arrowheads). *Inset* in *B* shows close-up of electrode tip. (*C*) Coronal striatal section (increased KChIP expression) in M1, displaying putative track and tip (arrowhead and close-up *Inset* on *Right*) of CF sensor in medial CN.

Table S1. Dopamine measurements made over time across probes in M1

			Stimulated dopamine oxidation current (nA)				Rate (transients per minute)			
Postimplant days	Probe ID	Estimated total scans	Predrug	Postdrug	% Change	*P* value	Predrug	Postdrug	% Change	*P* value
61	cn1	85,800	0.628	1.507	139.8	0.0160	0.633	1.341	111.7	0.0026
63	cn2	227,700	0.734	1.359	85.2	0.0022	0.440	0.587	33.4	0.4741
64	cn1	384,450	0.338	0.660	95.0	0.0027	0.468	0.652	39.5	0.3528
64	cn2	384,450	0.623	1.842	195.9	0.0201	0.182	0.548	201.3	0.0136
106	cn1	1,756,475	0.140	0.440	214.3	0.0102	0.148	0.303	104.4	0.2646
106	cn3	1,457,975	0.233	0.648	177.5	0.1766	0.370	0.346	−6.6	0.9917
126	cn1	2,394,650					0.000	0.064	infinity	0.0000
126	cn3	2,096,150					0.145	0.304	110.6	0.1926

Values of stimulated dopamine oxidation current represent those plotted in Fig. 2, and the *P* values are calculated using a paired *t* test. Rates of detected dopamine signals represent those plotted in Fig. 4, and the *P* values are calculated using a χ^2 test.